

GT2011-46389

A New Hex-8 Finite Element For Gas Turbine Engine Fatigue Life Prediction

Wasim Tarar*

**National University of Sciences and Technology
Rawalpindi, Pakistan**

M.-H. Herman Shen

**The Ohio State University
Columbus, OH 43210, USA**

ABSTRACT

High cycle fatigue is the major governing failure mode in aerospace structures and gas turbine engines. Different design tools are available to predict number of cycles to failure for a component subjected to fatigue loads. An energy-based fatigue life prediction framework was previously developed in recent research for prediction of axial, bending and torsional fatigue life at various stress ratios. The framework for the prediction of fatigue life via energy analysis was based on a new constitutive law, which states the following: the amount of energy required to fracture a material is constant. A 1-D ROD element for uniaxial fatigue, a BEAM element for bending fatigue and a QUAD-4 element for biaxial fatigue were developed by authors based on this constitutive law. In this study, the energy expressions that construct the new constitutive law are integrated into minimum potential energy formulation to develop a new HEX-8 BRICK finite element for fatigue life prediction. The newly developed HEX-8 BRICK element has 8 nodes and each node has 3 degrees of freedom (DOF) in x , y and z directions. This element is further modified to add the rotational and bending DOFs for application to real world three dimensional (3D) structures and components. HEX-8 BRICK fatigue finite element has capability to predict the number of cycles to failure for 3-D objects subjected to multiaxial stresses. The new HEX-8 element is benchmarked with previously developed uniaxial tension/compression finite element in order to verify the new development. The comparison of finite element method (FEM) results to existing experimental fatigue data, verifies the new finite element development for fatigue life prediction. The final output of this finite element analysis is in the form of number of cycles to failure for each element in ascending or descending order. Therefore, the new finite element framework can predict the number of cycles to failure at each location in gas turbine engine structural components. The new finite element provides a very useful tool for fatigue life prediction in gas turbine engine components as it provides a complete picture of fatiguing process. The performance of the HEX-8 fatigue finite element is demonstrated by comparison of life prediction results for Al6061-T6 to previously developed multiaxial fatigue life prediction approach by the authors. Another set of comparison is made to results for type 304 stainless steel data.

1. INTRODUCTION

Fatigue is the governing failure mode in rotating machinery components and structures subjected to cyclic loads. Most of the gas turbine engine blades are designed to be failure free; however, failure does occur and is commonly linked to fatigue. High cycle fatigue (HCF) is the main cause of failure in gas turbine engines [1]. Different design tools are available to analyze and determine the fatigue life. Stress versus cycles plot, or S-N curve is the most commonly used such tool. These curves provide fatigue strength with respect to cycles to failure. Other common tools for predicting fatigue properties are the Goodman diagram and the advanced Goodman diagram [2]. These diagrams are the popular choices for a failure-free aircraft engine design. In order for designers to make an accurate assessment, the applied cyclic loads are converted to equivalent stress and compared to S-N curve or Goodman diagram to obtain the number of cycles to failure. Most of data available in the form of these diagrams are based on uniaxial test data. It is sometimes seen: instead of uniaxial data, bench test data using components or blades also includes multiaxial results. This has led to search for a more realistic method for design comparison than the existing uniaxial design tools, which begins by observing the association between material failure/fracture and the energy dissipated during the process.

Scientists and engineers have tried since 1940's to relate energy conversion to fatigue life prediction of the material. These attempts resulted in minimal success [3]. The hypothesis used in this type of research implies: under cyclic loading or any bending, there exists a critical energy value for which failure occurs [4]. The continued research in this area later justified this hypothesis by displaying agreement between the theoretical and the experimental results on S-N curve. Further investigation of the assumption made in [4] led to the introduction of a correlation between the fatigue life of a material and the strain energy dissipation during the process [3, 5]. It is now believed that the strain energy required to fracture a material, monotonically, is the same as the strain energy during a cyclic fatigue procedure. Thus the critical energy value for each material is the monotonic strain energy. Based on this constitutive law, an improved energy-based criterion has been developed in recent research to allow one to systematically determine fatigue life based on the amount of energy loss per fatigue cycle [6-10]. The research [6-10] includes a vibration

* Corresponding Author: wasim6@gmail.com (Wasim Tarar)

based test method for fatigue life data acquisition and a new failure criterion. The thought behind the vibration-based methodology is supplying a dynamic base excitation to a specimen at a specified high resonant frequency, between 1200-1600 Hz, showing bending behavior. This testing method provides a significantly faster means for acquiring 10^6 cycles (between 10 & 14 minutes), therefore making it a more efficient means for acquiring HCF based on uniaxial conditions. The new failure criterion [6] includes stress-strain relationship both for monotonic as well as cyclic loadings. This failure criterion is further used to develop fracture energy and cyclic energy expression. These expressions are used to determine the failure energy and energy dissipated per cycle. Comparison of total fracture energy to cyclic energy dissipated per cycle yields the number of cycles to failure.

The previous research [11-15] by authors includes a development of a uniaxial 1-D rod, a bending beam element and a Quadrilateral 2-D element for uniaxial, bending and biaxial fatigue life prediction respectively. These elements are developed by integration of failure criterion presented in [6, 10] into minimum potential energy formulation. The rod, beam and QUAD-4 fatigue elements provide a useful tool for fatigue life prediction in gas turbine engine structural components. The accurate prediction of number of cycles with these new finite elements method and a good match of results to experimental data and analytical results [11, 15] signifies that the new finite element provides an estimation of number of cycles for axial and biaxial loading with sufficient accuracy. A multiaxial equivalent stress approach combining the energy methods and conventional fatigue finite element analysis procedure has also been developed [16].

This study presents the development of an eight-node Hexahedral (HEX-8) fatigue element. The constitutive equations presented by energy-based framework developed in [6, 10] are integrated into a minimum potential energy expression to develop the eight-node HEX element. This element has the capability to predict the number of cycles to failure for components subjected to stresses in x , y and z directions. The element is benchmarked with the previously developed uniaxial tension/compression solution [11] in order to verify the new development. The benchmarking procedures are discussed in detail in Section 3.

The newly developed HEX-8 Brick element is further modified by adding the extra degrees of freedom of a beam element to obtain the rotational capability. With these added rotational degrees of freedom, the HEX-8 Brick element can be used to model the 3-D structures subjected to multiaxial fatigue loads. The analysis of a Curved Plate, a turbine blade like structure, is performed using the new HEX-8 element. The results are compared to the equivalent stress approach analysis results presented in [16]. Another set of comparison is made to results for type 304 stainless steel [17, 18].

The output from the analysis with HEX-8 fatigue element is plotted in the form of a colored contour plot where different colors represent the number of cycles to failure for each element depending upon the varying stress at different locations. Due to the discrete nature of finite element method,

the new analysis approach can provide the number of cycles to failure for each element in the structure.

The commercial finite element tools like ANSYS and MSC.NASTRAN involve a process of obtaining the vibratory stresses through dynamic analysis and using the Goodman diagram and modified Goodman diagram to predict the fatigue life. This approach does not incorporate the fatiguing process in the analysis procedure. The new finite elements developed in [11-15] and new HEX-8 element presented in this study are based on a fatigue constitutive law developed in [6, 10]. Therefore, the analysis through these elements directly incorporates the fatiguing process in finite element analysis in order to obtain stresses and ultimately capture the energy dissipated due to fatigue cycles. The difference of approach between conventional finite element analysis and the new finite element procedure developed in [11-15] and this study is discussed in detail in Section 4.

2. BIAXIAL DATA FOR FATIGUE TESTS ON TYPE 304 STAINLESS STEEL

References [17, 18] present fatigue data on a specimen shown in Figure 1. The material of the specimen is type 304 stainless steel. The specimen is subjected to Tension-Torsion loading conditions. The experimental procedures are discussed in [17, 18] in detail. The stress-strain and S-N data are shown in Figures 2 and 3.

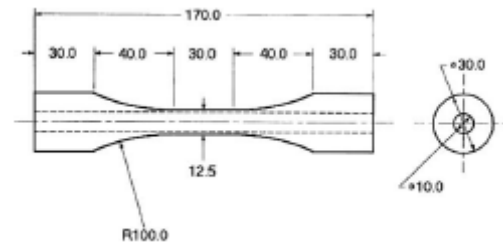


Figure 1: The Geometry of the Specimen [17, 18]

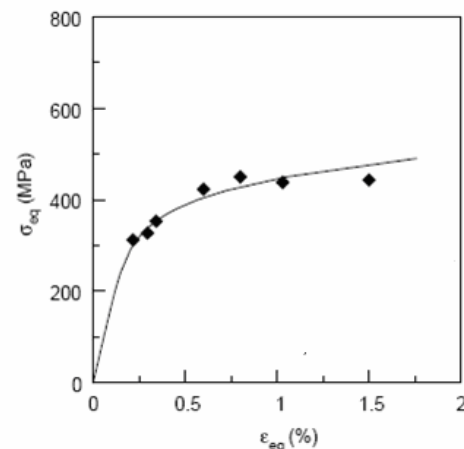


Figure 2: Stress-Strain Experimental Data for Type 304 Stainless Steel [17, 18]

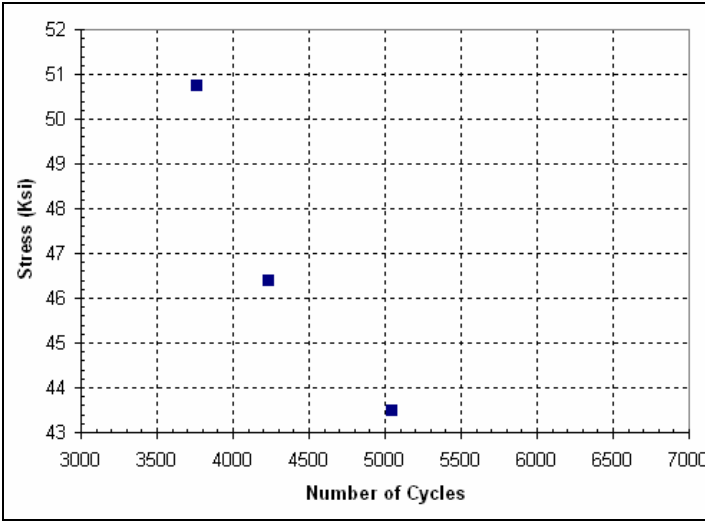


Figure 3: Fatigue Life Prediction Experimental Data for Type 304 Stainless Steel [17, 18]

3. DEVELOPMENT OF NEW HEX-8 FATIGUE ELEMENT

The procedures followed for development of new HEX-8 element are similar to presented by authors in [11-15] for development of uniaxial rod, beam and QUAD-4 fatigue elements.

The following Equations present the uniaxial and shear constitutive laws [6, 10] both for uniaxial monotonic and cyclic loadings respectively.

$$\varepsilon_{monotonic} = \frac{\sigma}{E} + \varepsilon_0 \sinh\left(\frac{\sigma}{\sigma_0}\right) \quad (1)$$

$$\varepsilon_{cyclic} = \frac{\sigma_{PP}}{E} + \frac{1}{C} \sinh\left(\frac{\sigma_{PP}}{\sigma_c}\right) \quad (2)$$

Equations 3 and 4 represent stress-strain relationships for shear monotonic and cyclic loads respectively [10].

$$\gamma_{monotonic} = \frac{\tau}{G} + \gamma_0 \sinh\left(\frac{\tau}{\tau_0}\right) \quad (3)$$

$$\gamma_{cyclic} = \frac{\tau_{PP}}{G} + \frac{1}{C_s} \sinh\left(\frac{\tau_{PP}}{\tau_c}\right) \quad (4)$$

Where the parameters displayed in Equations 1-4 are defined as follows: σ is the value for stress at the surface of the specimen (in the bending case, max stress), ε and γ are the strain corresponding to the stress σ and τ , σ_{pp} and τ_{pp} is the peak to peak stress (2σ when stress ratio is -1.0), E is the modulus of elasticity, and the variables σ_c , σ_0 , ε_0 , C , τ_c , τ_0 , γ_0 and C_s are curve fit parameters [10].

As is evident from Equations 1-4, the stress-strain relationships consist of two parts: linear elastic and a non-linear plastic expression. Integration of elastic part into minimum potential energy formulation is a classical finite element problem and is available in literature [19, 20].

Integration of non-linear parts of constitutive law is presented below.

If a three dimensional (3-D) stress tensor is defined as following,

$$\{\sigma_{ij}\} = \begin{bmatrix} \sigma_{xx} & \tau_{xy} & \tau_{xz} \\ \tau_{yx} & \sigma_{yy} & \tau_{yz} \\ \tau_{zx} & \tau_{zy} & \sigma_{zz} \end{bmatrix} \quad (5)$$

The corresponding stress elements for plastic part of Equations 1 to 4 are given by the following equations.

$$\sigma_{pm-xx} = \sigma_0 \sinh^{-1}\left(\frac{\varepsilon_{px}}{\varepsilon_0}\right) \quad (6)$$

$$\sigma_{pm-yy} = \sigma_0 \sinh^{-1}\left(\frac{\varepsilon_{py}}{\varepsilon_0}\right) \quad (7)$$

$$\sigma_{pm-zz} = \sigma_0 \sinh^{-1}\left(\frac{\varepsilon_{pz}}{\varepsilon_0}\right) \quad (8)$$

$$\tau_{pm-yz} = \tau_0 \sinh^{-1}\left(\frac{\gamma_{pyz}}{\gamma_0}\right) \quad (9)$$

$$\tau_{pm-xz} = \tau_0 \sinh^{-1}\left(\frac{\gamma_{pxz}}{\gamma_0}\right) \quad (10)$$

$$\tau_{pm-xy} = \tau_0 \sinh^{-1}\left(\frac{\gamma_{pxy}}{\gamma_0}\right) \quad (11)$$

The subscripts pm designate the plastic case for monotonic loading. An eight-node HEX element is shown in the following figure. The element has eight nodes with each node having three degrees of freedom, displacements in x , y and z directions.

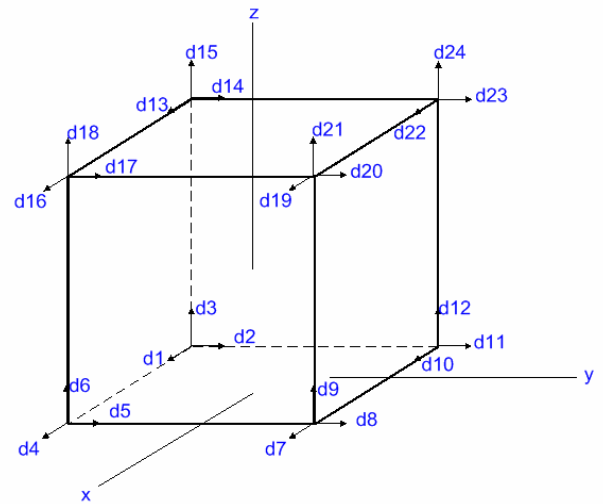


Figure 4: An Eight Node Hexahedral Element

The nodal displacement vector is denoted by d and d_s are x , y and z displacements at each node. The displacement at any point within the element is denoted by $u = [u(x,y,z), v(x,y,z), w(x,y,z)]^T$.

$$d = [d_1, d_2, d_3, \dots, d_{22}, d_{23}, d_{24}]^T \quad (12)$$

As stated earlier, the procedure followed for development of new HEX-8 fatigue element are similar to presented by the authors in [11-15]. HEX-8 element shown in Figure 4 is represented in $\xi - \eta - \zeta$ coordinates or natural coordinates and is brick shaped. These displacements are approximated using the Lagrange shape functions which satisfy nodal value and continuity requirements.

Integration of Equation 5 into Equation 13 provides new K-matrix for the plastic part of the fatigue constitutive.

$$\Pi = \int \sigma^T \varepsilon dV - \int u f dV - \int u T dx - \sum u_i P_i \quad (13)$$

Where Π is the minimum potential energy, σ is the stress tensor, ε is the strain vector, u is the displacement, f is the body force, T is the traction force, and P_i is the point load. V is the volume and x denotes the length of the element.

HEX-8 K-Matrices for linear elastic and non-linear plastic parts are represented by the following equations.

$$K_{em-Brick} = \int_{-1}^1 \int_{-1}^1 \int_{-1}^1 [k_{ij}] d\xi d\eta d\zeta \quad (14)$$

for $i = 0, \dots, 24$ and $j = 0, \dots, 24$

$$K_{pm-Brick} = \int_{-1}^1 \int_{-1}^1 \int_{-1}^1 [k_{ijpm}(d)] d\xi d\eta d\zeta \quad (15)$$

for $i = 0, \dots, 24$ and $j = 0, \dots, 24$

Where subscripts em and pm denote the elastic and plastic cases respectively. The elements of Kpm-Brick are given in the following Equations.

$$k_{ij-pm} = \frac{1}{8} \left[\frac{Q_i S_{ij} Q_j}{R_{11}} \right] \quad \text{for } i = 1, 4, 7, \dots, 22 \text{ and } j = 1, 4, 7, \dots, 22 \quad (16)$$

$$k_{ij-pm} = \frac{1}{8} \left[\frac{Q_i S_{ij} Q_j}{R_{12}} \right] \quad \text{for } i = 2, 5, 8, \dots, 23 \text{ and } j = 2, 5, 8, \dots, 23 \quad (17)$$

$$k_{ij-pm} = \frac{1}{8} \left[\frac{Q_i S_{ij} Q_j}{R_{12}} \right] \quad \text{for } i = 2, 5, 8, \dots, 23 \text{ and } j = 2, 5, 8, \dots, 23 \quad (18)$$

$$k_{ij-pm} = \frac{1}{8} \left[\frac{Q_i S_{ij} Q_j}{R_{12}} \right] \quad \text{for } i = 1, 4, 7, \dots, 22 \text{ and } j = 2, 5, 8, \dots, 23 \quad (19)$$

$$k_{ij-pm} = \frac{1}{8} \left[\frac{Q_i S_{ij} Q_j}{R_{13}} \right] \quad \text{for } i = 1, 4, 7, \dots, 22 \text{ and } j = 3, 6, 9, \dots, 24 \quad (20)$$

$$k_{ij-pm} = \frac{1}{8} \left[\frac{Q_i S_{ij} Q_j}{R_{11}} \right] \quad \text{for } i = 2, 5, 8, \dots, 23 \text{ and } j = 1, 4, 7, \dots, 22 \quad (21)$$

$$k_{ij-pm} = \frac{1}{8} \left[\frac{Q_i S_{ij} Q_j}{R_{13}} \right] \quad \text{for } i = 2, 5, 8, \dots, 23 \text{ and } j = 3, 6, 9, \dots, 24 \quad (22)$$

$$k_{ij-pm} = \frac{1}{8} \left[\frac{Q_i S_{ij} Q_j}{R_{11}} \right] \quad \text{for } i = 3, 6, 9, \dots, 24 \text{ and } j = 1, 4, 7, \dots, 22 \quad (23)$$

$$k_{ij-pm} = \frac{1}{8} \left[\frac{Q_i S_{ij} Q_j}{R_{12}} \right] \quad \text{for } i = 3, 6, 9, \dots, 24 \text{ and } j = 2, 5, 8, \dots, 23 \quad (24)$$

Where Q_i , Q_j , S_{ij} , R_{11} , R_{12} and R_{13} are given in the following table.

Table 1: Constants for Equations 16 to 24

i / j	Q_i / j	S_{ij}	R_{11}, R_{12} and R_{13}
1	$-\frac{2}{L}(1-\eta)(1-\zeta)$	$S_{ij} = \sigma_0 \sinh^{-1} \left(\frac{\varepsilon_{px}}{\varepsilon_0} \right)$ for $i = 1, 4, 7, \dots, 22$ and $j = 1, 4, 7, \dots, 22$	$R_{11} = \frac{2}{L} \begin{pmatrix} -(1-\eta)(1-\zeta)d_1 \\ +(1-\eta)(1-\zeta)d_4 \\ +(1+\eta)(1-\zeta)d_7 \\ -(1-\eta)(1-\zeta)d_{10} \\ -(1-\eta)(1+\zeta)d_{13} \\ +(1-\eta)(1+\zeta)d_{16} \\ +(1+\eta)(1+\zeta)d_{19} \\ -(1+\eta)(1+\zeta)d_{22} \end{pmatrix}$
2	$-\frac{2}{W}(1-\xi)(1-\zeta)$		
3	$-\frac{2}{H}(1-\xi)(1-\eta)$		
4	$\frac{2}{L}(1-\eta)(1-\zeta)$	$S_{ij} = \sigma_0 \sinh^{-1} \left(\frac{\varepsilon_{py}}{\varepsilon_0} \right)$ for $i = 2, 5, 8, \dots, 23$ and $j = 2, 5, 8, \dots, 23$	
5	$-\frac{2}{W}(1+\xi)(1-\zeta)$		
6	$-\frac{2}{H}(1+\xi)(1-\eta)$		
7	$\frac{2}{L}(1+\eta)(1-\zeta)$	$S_{ij} = \sigma_0 \sinh^{-1} \left(\frac{\varepsilon_{pz}}{\varepsilon_0} \right)$ for $i = 3, 6, 9, \dots, 24$ and $j = 3, 6, 9, \dots, 24$	
8	$\frac{2}{W}(1+\xi)(1-\zeta)$		

Continued

Table 1 Continued

Table 1: Constants for Equations 16 to 24

i/j	$Q_{i/j}$	S_{ij}	R_{11}, R_{12} and R_{13}
9	$-\frac{2}{H}(1+\xi)(1+\eta)$	$S_{ij} = \tau_0 \sinh^{-1} \left(\frac{\varepsilon_{pxy}}{\varepsilon_0} \right)$ for $i = 1, 4, 7, \dots, 22$ and $j = 2, 5, 8, \dots, 23$	$R_{12} = \frac{2}{W} \begin{pmatrix} -(1-\xi)(1-\zeta)d_2 \\ -(1+\xi)(1-\zeta)d_5 \\ +(1+\xi)(1-\zeta)d_8 \\ +(1-\xi)(1-\zeta)d_{11} \\ -(1-\xi)(1+\zeta)d_{14} \\ -(1+\xi)(1+\zeta)d_{17} \\ +(1+\xi)(1+\zeta)d_{20} \\ +(1-\xi)(1+\zeta)d_{23} \end{pmatrix}$
10	$-\frac{2}{L}(1+\eta)(1-\zeta)$		
11	$\frac{2}{W}(1-\xi)(1-\zeta)$		
12	$-\frac{2}{H}(1-\xi)(1+\eta)$	$S_{ij} = \tau_0 \sinh^{-1} \left(\frac{\varepsilon_{pxz}}{\varepsilon_0} \right)$ for $i = 1, 4, 7, \dots, 22$ and $j = 3, 6, 9, \dots, 24$	
13	$-\frac{2}{L}(1-\eta)(1+\zeta)$		
14	$-\frac{2}{W}(1-\xi)(1+\zeta)$		
15	$\frac{2}{H}(1-\xi)(1-\eta)$	$S_{ij} = \tau_0 \sinh^{-1} \left(\frac{\varepsilon_{pxy}}{\varepsilon_0} \right)$ for $i = 2, 5, 8, \dots, 23$ and $j = 1, 4, 7, \dots, 22$	
16	$\frac{2}{L}(1-\eta)(1+\zeta)$		

Continued

Table 1 Continued

Table 1: Constants for Equations 16 to 24

i/j	$Q_{i/j}$	S_{ij}	R_{11}, R_{12} and R_{13}
17	$-\frac{2}{W}(1+\xi)(1+\zeta)$	$S_{ij} = \tau_0 \sinh^{-1} \left(\frac{\varepsilon_{pyz}}{\varepsilon_0} \right)$ for $i = 2, 5, 8, \dots, 23$ and $j = 3, 6, 9, \dots, 24$	$R_{13} = \frac{2}{H} \begin{pmatrix} -(1-\xi)(1-\eta)d_3 \\ -(1+\xi)(1-\eta)d_6 \\ -(1+\xi)(1+\eta)d_9 \\ -(1-\xi)(1+\eta)d_{12} \\ +(1-\xi)(1-\eta)d_{15} \\ +(1+\xi)(1-\eta)d_{18} \\ +(1+\xi)(1+\eta)d_{21} \\ +(1-\xi)(1+\eta)d_{24} \end{pmatrix}$
18	$\frac{2}{H}(1+\xi)(1-\eta)$		
19	$\frac{2}{L}(1+\eta)(1+\zeta)$		
20	$\frac{2}{W}(1+\xi)(1+\zeta)$	$S_{ij} = \tau_0 \sinh^{-1} \left(\frac{\varepsilon_{pxz}}{\varepsilon_0} \right)$ for $i = 3, 6, 9, \dots, 24$ and $j = 1, 4, 7, \dots, 22$	
21	$\frac{2}{H}(1+\xi)(1+\eta)$		
22	$-\frac{2}{L}(1+\eta)(1+\zeta)$		
23	$\frac{2}{W}(1-\xi)(1+\zeta)$	$S_{ij} = \tau_0 \sinh^{-1} \left(\frac{\varepsilon_{pyz}}{\varepsilon_0} \right)$ for $i = 3, 6, 9, \dots, 24$ and $j = 2, 5, 8, \dots, 23$	
24	$\frac{2}{H}(1-\xi)(1+\eta)$		

L and W are length and width of the element respectively. Similar equations are developed for cyclic loads. The resulting K-matrices are shown in the following equations.

$$K_{ec-Brick} = \int_{-1}^1 \int_{-1}^1 \int_{-1}^1 [k_{ij}] d\xi d\eta d\zeta \quad (25)$$

for $i = 0, \dots, 24$ and $j = 0, \dots, 24$

$$K_{pc-Brick} = \int_{-1}^1 \int_{-1}^1 \int_{-1}^1 [k_{ijpc}(d)] d\xi d\eta d\zeta \quad (26)$$

for $i = 0, \dots, 24$ and $j = 0, \dots, 24$

The elements of $K_{pc-Brick}$ are the same as given in Equations 16 to 24 except that the parameters σ_0 changes to σ_c , ε_0 changes

to $1/C$, τ_o changes to τ_c , γ_o changes to $1/C_s$ and the applied stress σ and τ change to peak to peak stress σ_{pp} and τ_{pp} .

Equations 15 and 26 are non-linear due to presence of “ ds ” in the resulting K-matrices. To account for the non-linear behavior, the Newton-Raphson iteration method is applied to the analysis [21-23]. These K-matrices are used in Equation 27 to determine the unknown degrees of freedom.

$$[K]\{d\} = \{F\} \quad (27)$$

In order to develop HEX-8 fatigue element with rotational capability, the HEX-8 element is modified to have additional degrees of freedom per node to include rotation. The Brick element developed in Equations 14, 15 and 25, 26 has 8 nodes with three translational degrees of freedom assigned to each node. The modified element is obtained by adding three rotational DOFs in x , y and z direction to each node. This modification provides the enhanced HEX-8 Brick element with translational as well as rotational capability. The procedures for developing the modified HEX-8 Brick element are the same as presented in [12] for obtaining QUAD-4 (Plate) element. Figure 5 shows the modified HEX-8 Brick element with 6 DOFs per node.

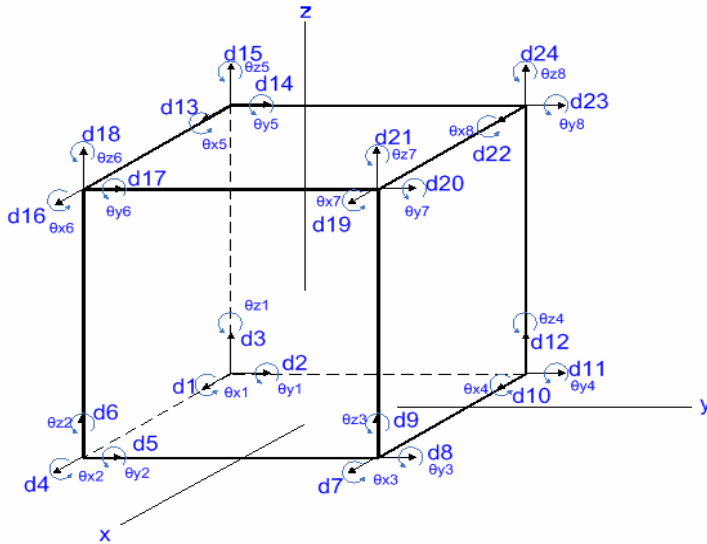


Figure 5: Modified HEX-8 Brick Element

The new HEX-8 Modified Brick element has the capability to model three dimensional components with all the translational and rotational degrees of freedoms. The Modified element is given by Equation 28.

$$K_{pm-Brick-Mod} = \begin{bmatrix} K_{pm-BrickPart} & O \\ O & K_{pm-BeamPart} \end{bmatrix} \quad (28)$$

4. FINITE ELEMENT PROCEDURES

A traditional HCF turbine blading system design procedure based on conventional fatigue life prediction approach is shown schematically in Figure 6. This design process usually consists of a structural dynamics analysis to determine natural frequencies and mode shapes at certain operating speed ranges and a stress analysis using a finite element based tool such as MSC NASTRAN and ANSYS [24-26] to calculate the dynamic stress distribution for identifying the maximum vibratory stress location or area under a series of given excitations. Once the maximum stresses for each vibration mode are determined, high cycle fatigue assessment can be achieved by measuring the margin between the maximum vibratory stress and the material fatigue capability which is a straight line drawn between the mean ultimate strength at zero vibratory stress and mean fatigue strength at 10^7 cycles (or infinite life). A typical Goodman diagram for the titanium alloy Ti-6Al-4V is shown in Figure 7 [27], constructed using uniaxial fatigue data.

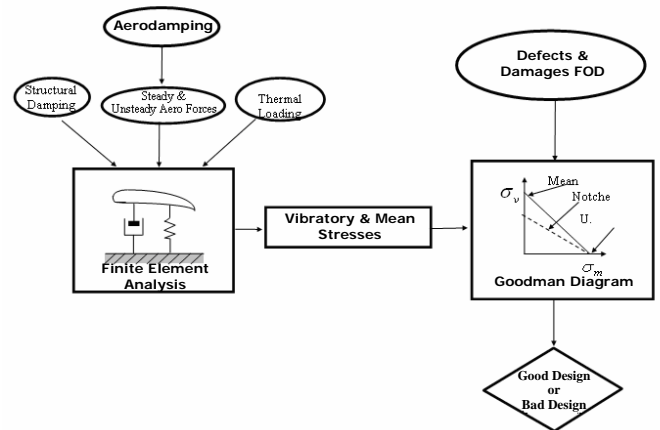


Figure 6: Conventional Finite Element Analysis approach to Fatigue Life Prediction

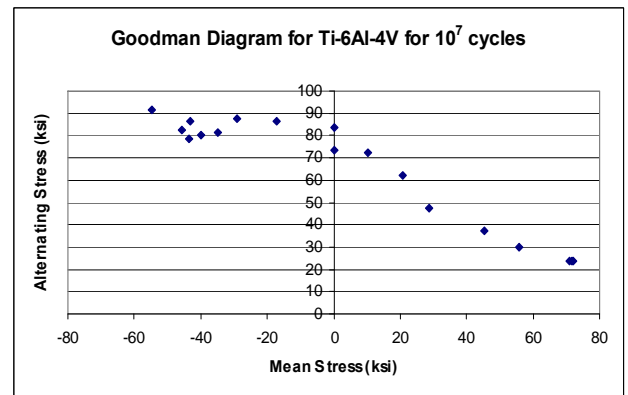


Figure 7: Typical Goodman (or Haigh) Diagram for Ti-6Al-4V for 10^7 cycles [27]

The analysis procedure developed for uniaxial rod and bending beam element involves application of cyclic loads and the process captures the energy dissipated for each cycle in the form of loading and unloading curves. These curves form a hysteresis loop and the area inside this loop provides energy dissipated per cycle [11, 12]. A similar procedure is adopted for analysis with new HEX-8 Brick element. The loads are applied

from 0 to peak to peak. The results are post-processed using classical FEA techniques. The nodal displacement results are further used to obtain stresses and strains for each element in the structure. The 3-D stresses and strains are converted to equivalent von-Mises stress and strain. These stresses and strains are used to calculate the energy dissipated per cycle and ultimately the number of cycles to failure for each element is obtained through comparison of cyclic energy to total fracture energy of the material. The calculations of energy and postprocessing procedures are the same as [11] for development of uniaxial rod fatigue element.

In order to verify the HEX-8 element, this element is benchmarked against the uniaxial rod element developed in [11]. A 3-D beam is meshed with the new HEX-8 elements and subjected to uniaxial tension in the x-direction in the form of displacement. The mesh discretization of this beam is shown in Figure 8. The displacement solution is compared to the solution of a 1-D bar meshed with the rod element and subjected to uniaxial tension. The beam and rod are fixed at left end and a unit displacement is applied at the right most end of rod and beam. The linear HEX-8 fatigue K-matrix results are compared to the linear 1-D rod solution as well as an ANSYS solution of the same problem.

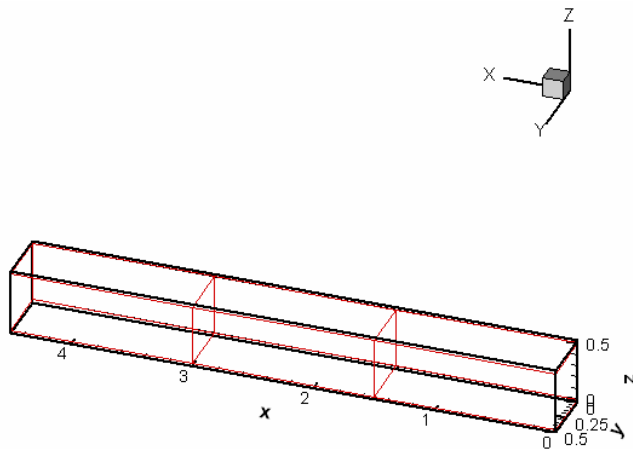


Figure 8: 3-Element Mesh for 3-D Beam (Dimensions in Inches)

The displacement results for linear verification from the HEX-8 element are shown in the following Figures and are compared in Table 2.

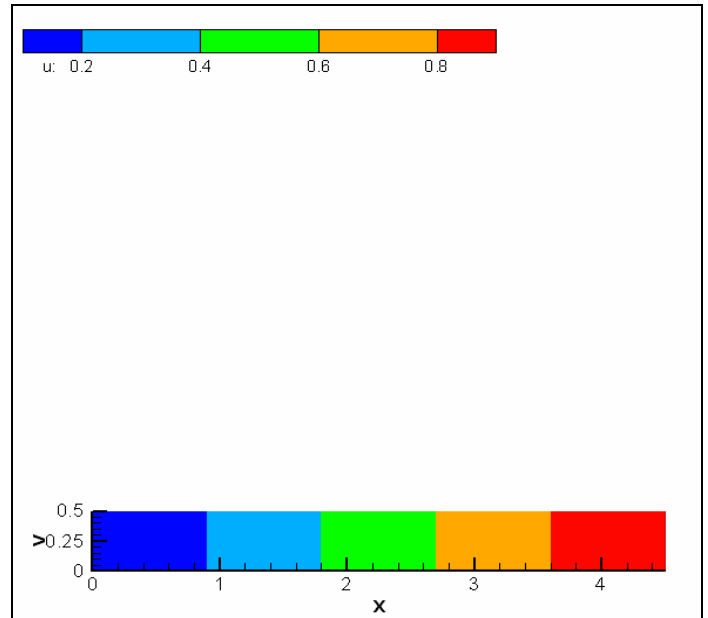


Figure 9: Displacement Results using HEX-8 Element (Dimensions in Inches)

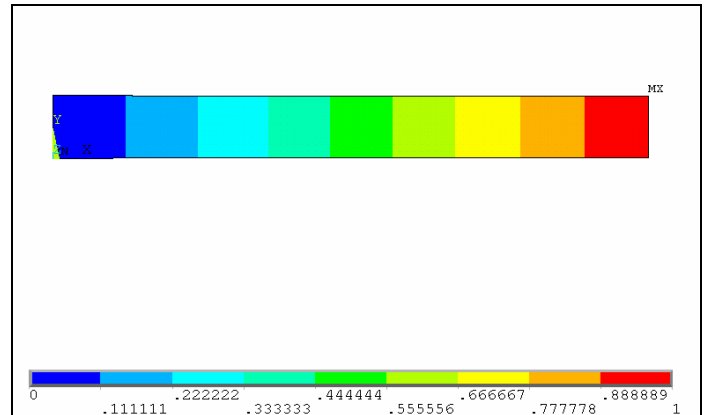


Figure 10: Displacement Results using HEX-8 Element in ANSYS (Dimensions in Inches)

Table 2: Linear Analysis Benchmarking of HEX-8 Element.

Node 2			Node 3			Node 4
1-D Bar (in)	ANSYS (in)	Linear Code HEX-8 (in)	1-D Bar (in)	ANSYS (in)	Linear Code HEX-8 (in)	(in)
0.333	0.333	0.333	0.666	0.666	0.6666	1.000

As stated earlier, the non-linear analysis requires an iterative approach. The non-linear HEX-8 Fatigue K-matrix results are compared to the linear 1-D rod solution. The results for non-linear analysis are shown in the following Figure and a tabular comparison is made in Table 3.

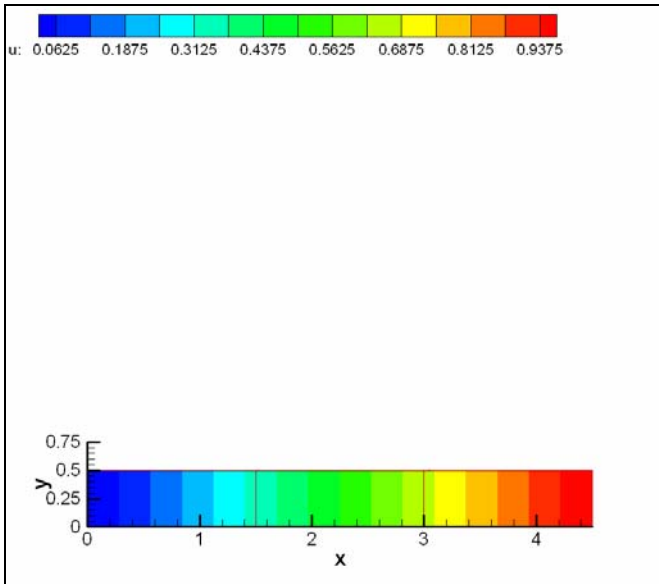


Figure 11: Displacement Results using Non-linear HEX-8 Fatigue Element (Dimensions in Inches)

Table 3: Non-Linear Analysis Benchmarking of HEX-8 Element.

Iteration No.	Node 2	
	Non-Linear Axial (in)	Non Linear 3D HEX-8(in)
1	0.0636458	0.0636162
2	0.0815309	0.0815113
5	0.1003474	0.1003213
9	0.1102611	0.1102112
10	0.1182828	0.1182121
12	0.1277408	0.1277129
35	0.2125675	0.2125277
49	0.3333354	0.3333911
Iteration No.	Node 3	
	Non-Linear Axial (in)	Non Linear 3D HEX-8(in)
1	0.1351291	0.1351901
2	0.1731019	0.1731111
5	0.2130519	0.2130125
9	0.2341001	0.2341112
10	0.2511314	0.2511192
12	0.2712119	0.2712105
35	0.4513112	0.4512145
49	0.6666702	0.6665117
Iteration No.	Node 4	
	Non-Linear Axial (in)	Non Linear 3D HEX-8(in)
1-49	1.0000	1.0000

As is evident from the results of Figure 9, 10 and 11 and the Tables 2 and 3, the HEX-8 fatigue element analysis compares exactly with the 1-D rod fatigue element. These results successfully complete the benchmarking of the new HEX-8 fatigue element. The analysis results performed using this element are presented in the following Section.

5. RESULTS AND DISCUSSION

The curved plate discussed in [16] is shown in the Figure below. This plate is discretized with HEX-8 Modified Brick elements. The plate is fixed at one end and is subjected to bending load at the other end. The analysis is performed to verify that the stress results and the fatigue life prediction with the new HEX-8 element correlate with each others.

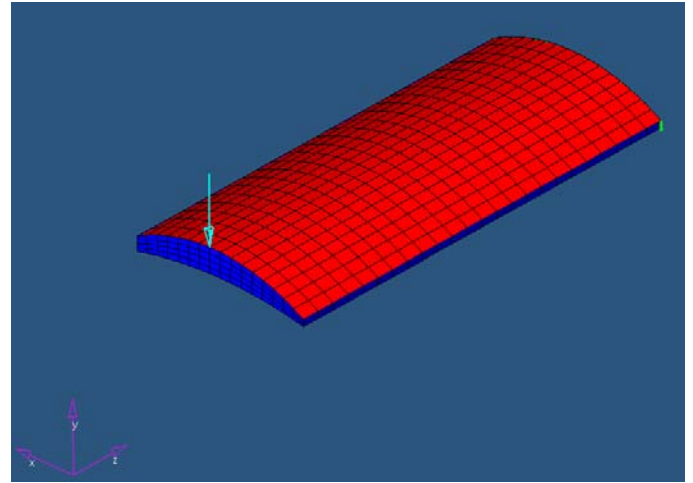


Figure 12: Curved Plate Meshed with Modified Brick Elements

The following Figures present the stress and fatigue life analysis results. The stresses are high in the area closer to the fixed end. The low fatigue life is predicted at the same locations where high stresses are present.

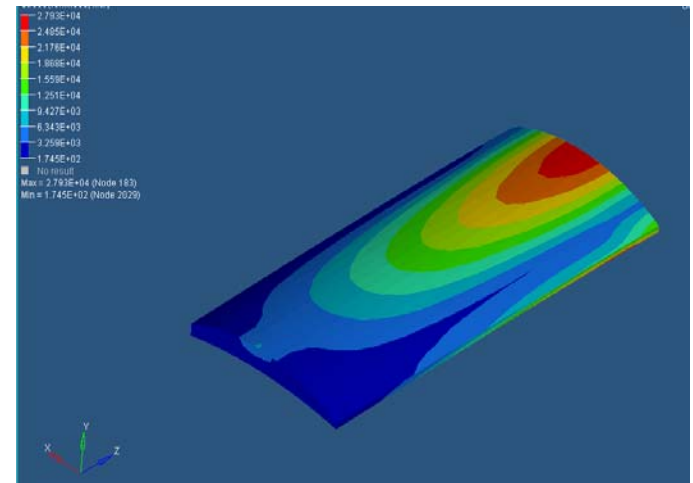


Figure 13: Stress Results with Modified Brick Elements (Psi)

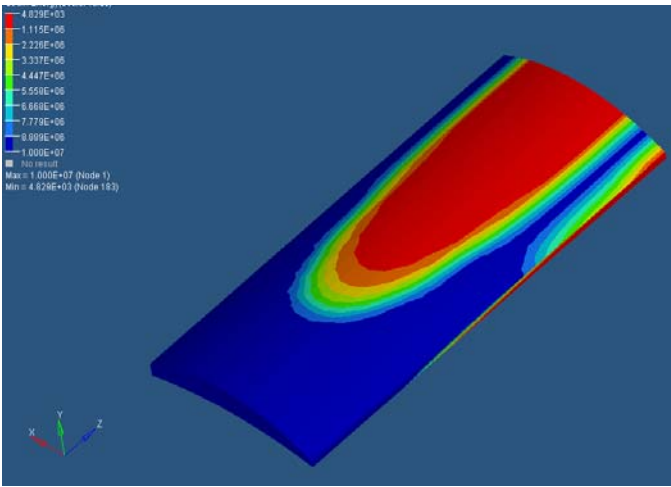


Figure 14: Fatigue Life Prediction with Modified Brick Elements

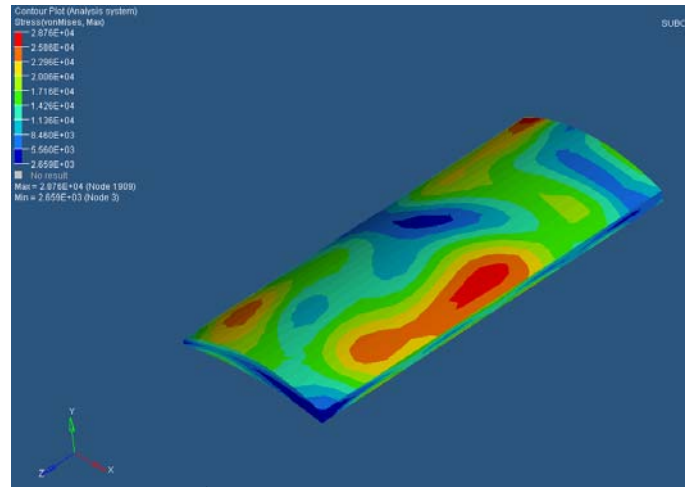


Figure 16: 3rd Stripe Mode Shape Stress Results (Psi) (Brick Element)

In order to have a comparison of results from analysis with the new brick element to those presented in [16], the curved plate meshed with the new brick element is excited to a stress level of 25 ksi for 3rd stripe mode and the stress and prediction results are compared to the equivalent stress approach prediction performed in [16]. Equation 27 is modified for this analysis for dynamic analysis [28] as given by Equation 29.

$$[M]\{\ddot{d}\} + [K]\{d\} = \{F \cos \omega t\} \quad (29)$$

Where M is the mass matrix and ω is the frequency. The displacement and stress contours from both the analysis match with each other and the maximum stresses are located away from the fixed end. The Figures 15-17 show the displacement, vibratory stress and the fatigue life prediction results, respectively, for this analysis.

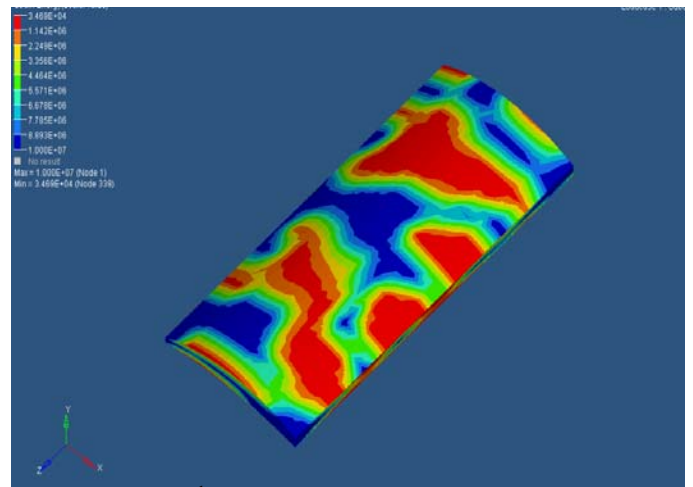


Figure 17: 3rd Stripe Mode Shape Fatigue Life Results (Brick Element)

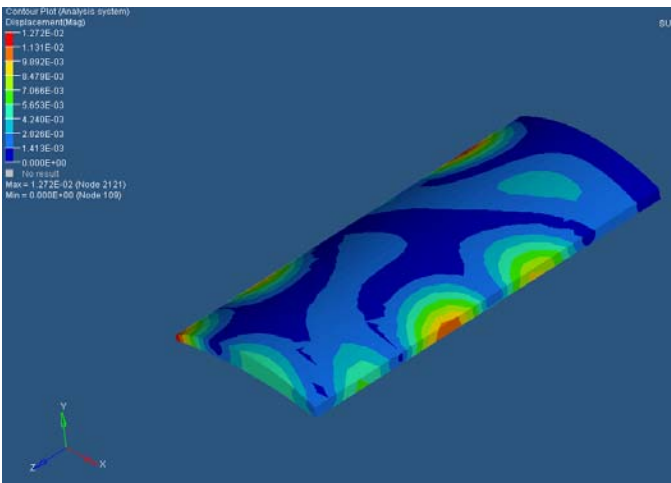


Figure 15: 3rd Stripe Mode Shape Results (Brick Element)

Table 4 shows a comparison of results from the vibration analysis performed on the curved plate meshed with the new Brick element. The results match well with the equivalent stress approach presented in [16].

Table 4: Comparison of Brick Element Results with Equivalent Stress Approach

	Stress (ksi)	FE Analysis Equivalent Stress Approach	FE Analysis Brick Element
Curved Plate	20	9.16 x E5	8.99 x E5

Another set of comparison is made for type 304 stainless steel experimental data [17, 18] discussed in Section 2, the equivalent stress fatigue life prediction performed in [16] and the fatigue analysis results performed using the new HEX-8 element. The results are shown in Figure 18 and a comparative data is presented in Table 5. The life prediction results performed using the HEX-8 element show a good match to the experiential data as well as equivalent stress approach.

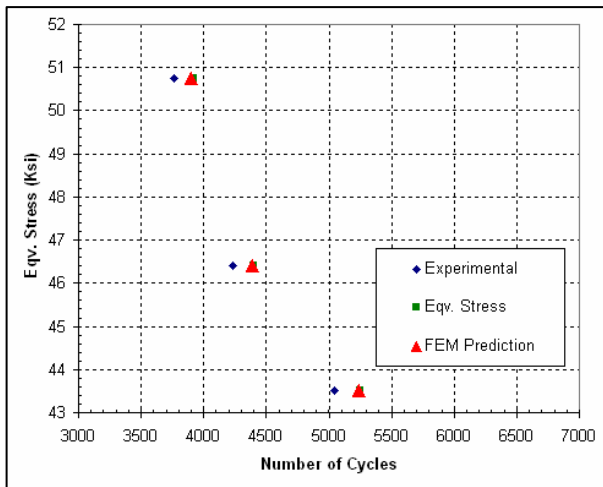


Figure 18: Comparison for Fatigue Life Prediction Results for Type 304 Stainless Steel

Table 5: Fatigue Results for Type 304 Stainless Steel

	Stress (ksi)	Life Cycles Experiment	Life Cycles Eqv. Stress	Life Cycles HEX-8	Percent Difference (%)
1	43.5	5044	5250	5235	3.79
2	46.4	4234	4401	4388	3.65
3	50.75	3767	3915	3904	3.64

The equivalent stress fatigue analysis discussed in [16] follows part of the conventional analysis approach [24-26] as it obtains the stresses through dynamic analysis using ordinary HEX-8 elements. When performing the analysis with the new fatigue element developed in this study, the mode shapes and stresses are obtained from direct analysis of the component meshed with the HEX-8 fatigue elements. Therefore, this analysis in comparison to equivalent stress approach skips multiple analysis steps and makes the prediction a one step procedure. Furthermore, the prediction results with the HEX-8 fatigue elements show closer comparison to experimental results as compared to the equivalent stress approach.

6. CONCLUSIONS

The newly developed HEX-8 (Brick) and Modified Brick elements provide useful tool for multiaxial fatigue life prediction. The results presented in Section 5 show that the new Brick element can predict the fatigue life in gas turbine engine structural component with improved accuracy. As these elements are developed from the energy-based constitutive law for fatigue life prediction, analysis with these elements directly incorporates the fatigue mechanism into fatigue analysis. Due to the discrete nature of finite element analysis, new fatigue elements can predict number of cycles to failure at each location in a component. The capability of HEX-8 element to predict varying fatigue life can provide visual picture of fatiguing process across the component. As in the case of uniaxial and QUAD-4 elements, the new HEX-8 elements developed in this study predict crack initiation whereas most research in this area [29-35] is related to crack propagation. This fact, along with integration of the fatigue constitutive law into the fatigue analysis mechanism, establishes the difference of the newly developed HEX-8 element from the existing fatigue FEA software and related research.

ACKNOWLEDGEMENTS

The authors would like to thank the Air Force Research Laboratory, Propulsion Directorate at Wright-Patterson Air Force Base, Ohio for their financial support and encouragement of this research.

REFERENCES

- Nicholas T. (1999). "Critical Issues in High Cycles Fatigue". *Int. J. Fatigue*, **21**, 221-231.
- Goodman J. (1899). "Mechanics Applied to Engineering". Longmans, Green, and Co., London.
- Feltner C. E. and Morrow J. D. (1960). "Micro Plastic Strain Hysteresis Energy as a Criterion for Fatigue Failure". American Society of Mechanical Engg. Paper No. 60-MET-2.
- Enomoto N. (1955). "On Fatigue Tests under Progressive Stress". **55**, American Society for Testing and Materials, 903.
- Stowell E. (1996). "A Study of the Energy Criterion for Fatigue". *Nuclear Eng. Design*, **3**, 32-40.
- Scott-Emuakpor O., Shen M.-H. H., Cross C., Calcaterra J., and George T. (2007). "Development of an Improved High Cycle Fatigue Criterion". *J. Eng. Gas Turbines and Power*, **129**, 162-169.
- George T., Seidt J., Shen M.-H. H., Cross C., and Nicholas T. (2004). "Development of a Novel Vibration-Based Fatigue Testing Methodology". *Int. J. Fatigue*, **26** (5), 477-486.
- George T., Shen M.-H. H., Scott-Emuakpor O., Cross C., Nicholas T., and Calcaterra J. (2005). "Goodman Diagram Via Vibration-Based Fatigue Testing". *J. Eng. Mater. Technol.*, **127** (1), 58-64.
- George T., Shen M.-H. H., Cross C. and Nicholas T. (2006). "A New Multiaxial Fatigue Testing Method for Variable-Amplitude Loading and Stress Ratio". *J. Eng. Gas Turbines Power*, **128**, 857-864.
- Scott-Emuakpor O., (2007) "Development of a Novel Energy Based Method for Multiaxial Fatigue Strength Assessment." Ph.D. Dissertation, The Ohio State University.
- Tarar W., Scott-Emuakpor O., Shen M.-H. H., (2007). "A New Finite Element for Gas Turbine Engine Fatigue Life Prediction". IGTI GT2007-27427.
- Tarar W., (2008). "A New Finite Element Procedure for Fatigue Life Prediction and High Strain Rate Assessment of AHSS." PhD Dissertation, The Ohio State University.
- Tarar W., Shen M.-H. H., (2010). "A New Finite Element Approach to Biaxial Fatigue Life Prediction in Gas Turbine Engine". Prediction Procedure". IGTI GT2010-23095.
- Tarar W., Scott-Emuakpor O., Shen M.-H. H., (2010). "Development of New Finite Elements for Fatigue Life Prediction in Structural Components". *J. Struc. Engg. and Mech.* Volume 35, No.5.

15. Tarar W., Shen M.-H. H., George T., Cross C., (2010). "A New Finite Element Procedure for Fatigue Life Prediction of Al6061 Plates under Multiaxial Loadings". *J. Struc. Engg. and Mech.* Volume 35, No.6.
16. Tarar W., Scott-Emuakpor O., Shen M.-H. H., George T., Cross C., (2008). "A New Energy-Based Multiaxial Fatigue Life Prediction Procedure". IGTI GT2008-51170.
17. Jin D., Wu J. and Chen X., (2006). "Fatigue Life Prediction under Sequential Biaxial Loading." *Key Engg. Matr. Vols 324-325*.
18. Chen X., Jin D., Kim K.S., (2006). "Fatigue Life Prediction of Type 304 Stainless Steel under Sequential Biaxial Loading." *Int. J. Fatigue.* (28).
19. Reddy J.N., (1984). "An Introduction to the Finite Element Methods." McGraw-Hill Book Company, New York.
20. T.R. Chandrupatal and A.D. Belegunda, (2002). "Introduction to Finite Elements in Engineering." Prentice-Hall, Inc.
21. Reddy J.N., (2004). "An Introduction to Non-Linear Finite Element Analysis." Oxford University Press, New York.
22. Masud A., Khurram R.A., (2004) "A Multiscale Finite Element Method for the Incompressible Navier–Stokes Equations." *Computer Methods Appl Mech Engg.* 193, 21-22, 2004.
23. Khurram R.A., Masud A., (2006). "A Multiscale/Stablized Formulation of the Incompressible Navier–Stokes Equations for Moving Boundary Flows and Fluid Structure Interaction." *Computational Mech.* 38, 4-5.
24. LMS Engineering Innovations: <http://www.lmsintl.com>
25. Desktop Engineering (DE): <http://www.deskeng.com>
26. MSC Software: <http://www.mscsoftware.com>
27. Nicholas T. and Maxwell D. (2003). "Mean Stress Effects on the High Cycle Fatigue Limit Stress in Ti-6Al-4V." *Fatigue and Fracture Mechanics*, ASTM STP 1417."
28. Meirovitch L. "Fundamentals of Vibration." McGraw-Hill Companies
29. Sumi Y., Mohri M., Kawamura Y., (2005). "Computational Prediction of Fatigue Crack Paths in Ship Structural Details." *Fatigue Fract Engng Mater Struct* 28 (1-2), 107–115.
30. Salvini P., Cardecchia E., Emofonti G., (1997). "A Procedure for Fatigue Life Prediction of Spot Welded Joints." *Fatigue Fract Engng Mater Struct.* 20 (8), 1117–1128.
31. Fermér M., Svensson H., (2001). "Industrial Experiences of FE-Based Fatigue Life Predictions of Welded Automotive Structures." *Fatigue Fract Engng Mater Struct.* 24 (7), 489–500.
32. Papanikos P., Tserpes K. I., Pantelakis SP., (2003). "Modeling of fatigue damage progression and life of CFRP laminates." *Fatigue Fract Engng Mater Struct* 26 (1), 37–47.
33. Lee H.-J., Song J.-H. (2005). "Finite-Element Analysis of Fatigue Crack Closure under Plane Strain Conditions: Stabilization Behavior and Mesh Size Effect." *Fatigue Fract Engng Mater Struct.* 28 (3), 333–342.
34. Park S. -J, Earmme Y.-Y., Song J. -H. (1997). "Determination of the Most Appropriate Mesh Size for a 2-D Finite Element Analysis of Fatigue Crack Closure Behavior." *Fatigue Fract Engng Mater Struct.* 20 (4), 533–545.
35. Papanikos P., Meguid S. A. (1994). "Theoretical and Experimental Studies of Fretting-Initiated Fatigue Failure of Aero engine Compressor Discs." *Fatigue Fract Engng Mater Struct.* 17 (5), 539–550.